Regulation of podosome formation in aortic endothelial cells vessels by physiological extracellular cues

Florian Alonso, Pirjo Spuul, Marion Decossas, Isabel Egaña, Filipa Curado, Isabelle Fremaux, Thomas Daubon, Elisabeth Génot

▶ **To cite this version:**

Florian Alonso, Pirjo Spuul, Marion Decossas, Isabel Egaña, Filipa Curado, et al.. Regulation of podosome formation in aortic endothelial cells vessels by physiological extracellular cues. European Journal of Cell Biology, 2020, 99 (4), pp.151084. 10.1016/j.ejcb.2020.151084 . hal-03453982

HAL Id: hal-03453982
https://hal.science/hal-03453982

Submitted on 22 Aug 2022

HAL is a multi-disciplinary open access archive for the deposit and dissemination of scientific research documents, whether they are published or not. The documents may come from teaching and research institutions in France or abroad, or from public or private research centers.

L'archive ouverte pluridisciplinaire **HAL**, est destinée au dépôt et à la diffusion de documents scientifiques de niveau recherche, publiés ou non, émanant des établissements d'enseignement et de recherche français ou étrangers, des laboratoires publics ou privés.

Distributed under a Creative Commons Attribution - NonCommercial 4.0 International License

Version of Record: https://www.sciencedirect.com/science/article/pii/S0171933520300236
Manuscript_a06db44055e2c50a368218b56612ff37

Regulation of podosome formation in aortic endothelial cells vessels by physiological extracellular cues

Florian Alonso[a,b], Pirjo Spuul[a,b,1], Marion Decossas[a,c], Isabel Egaña[a,b,2], Filipa Curado[a,b,3], Isabelle Fremaux[a,b], Thomas Daubon[a,b,4], Elisabeth Génot[a,b] *

[a] Université de Bordeaux, F-33000 Bordeaux, France

[b] INSERM U1045, F-33000 Bordeaux, France

[c] CBMN, UMR 5248, F-33000 Bordeaux, France

[1] Present address: Department of Chemistry and Biotechnology Division of Gene Technology, Tallinn University of Technology, Akadeemia Rd 15, 12618 Tallinn, Estonia

[2] Present address: Oncomatryx Biopharma, Arteaga Auzoa, 43, 48160 Derio, Bizkaia, Spain

[3] Present address: Centogene AG, The Rare Disease Company, Am Strande 7, 18055 Rostock, Germany

[4] Present address: IBGC, UMR 5095, 146, rue Léo Saignat, 33 000, Bordeaux, France

*Corresponding author: Elisabeth Génot, IECB, inserm1045, 2 rue Robert Escarpit, 33 600 Pessac, France

Phone: +33 540 003 056

Mail: elisabeth.genot@inserm.fr

Key words: endothelial cells, extracellular matrix, cytoskeleton, podosomes, vascular biology

Abbreviations: EC, endothelial cells; BAE cells, bovine aortic endothelial cells; TGFβ, transforming growth factor β; TEM, transmission electron microscopy; WASp/N-WASp, Wiskott-Aldrich syndrome proteins; MT1-MMP, membrane type-1 metalloprotease; 2D, two-dimensional; 3D, three-dimensional; ECM, extracellular matrix; interference reflection microscopy (IRM).

© 2020 published by Elsevier. This manuscript is made available under the CC BY NC user license
https://creativecommons.org/licenses/by-nc/4.0/

Abstract

Invadosomes are specialised actin-based dynamic microdomains of the plasma membrane. Their occurrence has been associated with cell adhesion, matrix degrading and mechanosensory functions that make them crucial regulators of cell migration and invasion. Monocytic, cancer cell and Src-transformed cell invadosomes have been extensively described. Less well defined are the structures which form in other cell types, i.e., non-haematopoietic and non-transformed cells, exposed to specific stimuli. We herein describe the specificities of podosomes induced in aortic endothelial cells stimulated with TGFβ *in vitro* and in conditions that more closely resemble the *in vivo* situation. These podosomes display the typical architecture of monocytic podosomes. They organise into large rosette-shape superstructures where they exhibit collective dynamic behavior consisting in cycles of formation and regression. At the ultrastructural level, microfilament arrangements in individual podosomes were revealed. Oxygen levels and hemodynamic forces, which are key players in endothelial cell biology, both influence the process. In 3D environment, podosomes appear as globular structures along cellular extensions. A better characterization of endothelial podosomes has far-reaching implications in the understanding and, possibly, in the treatment of some vascular diseases.

1. Introduction

Podosomes and invadopodia (collectively known as invadosomes) are cell-matrix contact microdomains that significantly differ from other adhesion structures in terms of molecular composition and functions (Paterson and Courtneidge, 2018). Their occurrence either as isolated but interconnected entities or superstructures, has been associated with cell adhesion, matrix degrading and mechanosensory functions that make them crucial regulators of cell migration and invasion. One of the most distinctive features of these complex structures is their high content in metalloproteases (MMPs), endowing them with proteolysis capacities that contribute to extracellular matrix (ECM) remodeling. More recently, a mechanosensing function has been assigned to these structures with no description of the involvement of MMPs (van den Dries et al., 2019). Podosomes form spontaneously upon cell adhesion in several subsets of the myelomonocytic lineage such as osteoclasts, macrophages and immature dendritic cells (Linder and Aepfelbacher, 2003). In these cells, on a two-dimensional surface under *in vitro* conditions, podosomes are visualized as punctate dynamic bipartite microdomains of the ventral membrane (Alonso et al., 2019). The dense F-actin core structure is enriched in several actin-associated proteins (Cdc42, Arp2/3, cortactin/HS1, WASp, WIP, dynamin, gelsolin), which regulate actin polymerization perpendicularly to the substratum. Integrins and various signaling and adaptor proteins among which vinculin and paxillin, the tyrosine kinases Src and Pyk2 surround the core structure. This ring complex links cell surface integrins to an interconnected network of actin filaments radiating from the F-actin cores, allowing collective dynamical behaviors. On stiff substrata, podosomes extend upwards from the ventral cell surface into the cytoplasm. Characterization of podosomes in the orthogonal plane (perpendicular to the basal membrane) has

revealed the existence of another substructure, the podosome cap. It covers the column of actin filaments like an umbrella and contains proteins such as FMNL1 (formin-like protein), INF2 (inverted formin), SVIL (supervillin) and LSP1 (Lymphocyte specific protein 1) (Cervero et al., 2018). This structure may serve as a hub for incoming transport vesicles, regulate podosome growth or channel the myosin contractile forces associated with podosomes (Cervero et al., 2018). Podosome related structures called invadopodia are found in invasive cancer cells displaying aberrant signaling (Buccione et al., 2004). They appear as long filopodial-like membrane extensions that penetrate into the ECM. Invadopodia are also surrounded by adhesion rings that form during their maturation and correlate strongly with their proteolytic activity (Branch et al., 2012). Invadopodia are heterogeneous in size, less numerous than podosomes and often located in the perinuclear area in the vicinity of the golgi apparatus. Neither the cap substructure, nor the actomyosin inter-podosome network has been investigated at invadopodia.

Podosomes are also found in non-haematopoietic and non-transformed cells, such as megakaryocytes (Schachtner et al., 2013), trabecular meshwork cells (Aga et al., 2008; Han et al., 2013), extravillous trophoblasts (Patel and Dash, 2012), neural crest cells (Murphy et al., 2011), neuronal growth cones (Santiago-Medina et al., 2015), smooth muscle cells (Burgstaller and Gimona, 2004; Kaverina et al., 2003) and endothelial cells (ECs) (Rottiers et al., 2009; Varon et al., 2006). They are therefore potentially involved in a wide range of physiological processes that are now under investigation. Importantly, in non-myelomonocytic cells, podosomes are not detected in the quiescent state but appear under appropriate stimulation, which may be provided by cytokines, micro-RNAs, matrix signals, mechanical constraints or developmental cues (Curado et al., 2014; Paterson and Courtneidge, 2018; Spuul et al., 2015; Veillat et al., 2015). Inducible podosomes contain the well-known components of the core and ring moieties but a number of hematopoietic podosomal proteins such as WASp, Pyk2, HS1 or β2 integrins are represented by other family members more ubiquitously expressed, N-WASp, FAK, cortactin and β1 integrins, respectively (Calle et al., 2006). These components are also those found at invadopodia and Src-induced podosomes. Such differences in invadosome composition may impact on their formation, architecture, organization and dynamics.

Our recent studies have characterized the specific features of podosomes that are induced in microvascular ECs in response to the angiogenic factor VEGF (Vascular Endothelial cell Growth Factor). VEGF-induced podosomes breach the basement membrane, enabling the invasive step of angiogenesis (Spuul et al., 2016b). However, podosomes also form in ECs isolated from large vessels (Varon et al., 2006) and in aortic vessel explants (Rottiers et al., 2009) exposed to TGFβ but the pathophysiological significance of these observations remains unknown. Because of their unique localisation at the blood/tissue interface, ECs are exposed to various oxygen concentrations, which depend on the vessel considered. They are also exposed to flow laminar shear stress in straight vessel portions but to disturbed flow at vessel bifurcations. These parameters are key players in vascular

biology as they determine EC behavior that drive vessel remodeling to adapt to hemodynamic changes (Sho et al., 2002a).

In the present study, we have explored some of the specificities of podosome rosettes formed in aortic ECs exposed to TGFβ *in vitro* and analysed the influence of environmental conditions that more closely resemble the *in vivo* situation. Collectively, our observations indicate that this TGFβ is likely to be modulated by multiple extracellular cues *in vivo*.

2. Results and discussion

General and specific features of podosomes in aortic endothelial cells

On planar substrates, podosomes display a bipartite architecture that can easily be visualized by double staining where phalloidin highlights the F-actin core and vinculin labels the adhesive surrounding ring (Calle et al., 2006). In sparse cultures of bovine aortic endothelial cells (BAE cells), the double staining approach reveals podosomes in 5-30% of the cells after 24h stimulation with TGFβ (Varon et al., 2006). These podosomes are always organized in rosettes: rings and to a lesser extent, clusters (about 15 µm in diameter or smaller), and arise in a lamellipodia-like extension (Fig. 1A-C). Podosome rosette dynamics has been studied in detail in Src-transformed cells (Collin et al., 2006) and our observations suggested that endothelial podosomes also undergo spatial rearrangement over time. Time-lapse video microscopy was thus performed to examine F-actin dynamics in lifeact-mGFP-transfected BAE cells stimulated with TGFβ. Live-cell imaging of podosome rosettes revealed that the superstructure undergoes successive cycles consisting in the emergence of a cluster of podosomes that grew and expand to develop in a ring that subsequently shrank and collapsed until the rosette reformed for another cycle (Fig. 1D and movie 1). Several cycles of around 10 min each were observed (average cycle was 11 min 40 sec ± 1 min 40 sec) and this dynamic and periodic behavior was observed for all rosettes analysed (n= 10). During the entire recording time, cells were immobile. The average diameter of the formed podosome rosettes during live cell imaging was 14.73 µm ± 2.3 µm. Formation of podosome rosettes was also analysed with interference reflection microscopy (IRM) showing that the whole area of the podosome rosette is close to glass coverslip during the entire cycle (Suppl. Fig 1). Collectively, these results reveal that the various patterns of podosome rosettes observed in fixed BAE cells represent the continuum of a dynamic behavior of the superstructure visualized by videomicroscopy. When BAE cells were seeded onto fluorescent gelatin to visualize podosome rosette proteolytic activity upon stimulation with TGFβ, the average diameter of degraded areas was 18.09 µm ± 6.9 µm (n=68 rosettes). Some degraded areas were found under the podosome rosettes stained with F-actin (Suppl. Fig. 2A). The degradation index of BAE cells was strongly increased by TGFβ (Suppl. Fig. 2B). These results confirm the dynamic behavior of the rosettes degrading the underlying matrix. In Src transformed cells and osteoclasts, the cluster-to-ring is regulated by FAK interactions with p130 Cas whereas podosome ring disassembly is controlled by an increase of Rho/ROCK activity and actomyosin-based contraction (Pan et al., 2011). Future studies will establish if the process is

regulated by these pathways in ECs. In ECs, podosome rosette life span, size and shape appear more constant and regular as compared to podosome rosettes formed by v-Src-transformed cells (Kuo et al., 2018).

Although gelatin is commonly used for its convenience as a readout of podosome activity, most ECM substrata seem to be permissive to podosome formation (Labernadie et al., 2010; van den Dries et al., 2012). However, some ECM proteins appear more favorable than others. For example, vitronectin is the preferred substrate for osteoclast podosomes (Fuller et al., 2010) whereas fibrinogen is the favorite one for macrophages (Labernadie et al., 2010). In the quiescent vessel, ECs rest on the basement membrane which plays a critical role in stabilizing the vasculature. However, in pathological settings, fibronectin and collagen I may accumulate in the vessel wall. ECs can therefore be exposed to diverse ECM microenvironnement *in vivo*. When BAE cells were seeded on various ECM components, podosome rosettes were formed on all the matrices analysed upon TGFβ stimulation (Fig. 1E). Some ECM proteins, specifically Collagen I, modulated the podosome response significantly compared to the glass condition. However, it should be noted that similarly to smooth muscle cells, BAE cells are known to produce ECM proteins and their synthesis is strongly stimulated by TGFβ (Basson et al., 1992). Therefore, the effect of the ECM coating may be influenced by BAE-derived ECM accumulating during the stimulation period (extended as podosome formation requires protein synthesis (Varon et al., 2006)). Interestingly, none of the matrices tested affected the podosome response in non-stimulated cells. Thus, it is likely that *in vivo*, the ECM microenvironment contributes to podosome formation in aortic ECs exposed to TGFβ.

Endothelial podosomes are interconnected within the rosettes

The collective behavior of podosome clusters reflects in their interconnection that was demonstrated by ultrastructural and super-resolution imaging techniques in macrophages, immature dendritic cells and osteoclasts (Akisaka et al., 2008; Labernadie et al., 2010; Luxenburg et al., 2012; van den Dries et al., 2013). Using a correlative approach, combining transmission electron microscopy (TEM) with fluorescence microscopy on the same sample, we visualized the architecture of the rosettes formed in BAE cells (Fig. 2). Under conventional conditions of fixation and staining, podosome rosettes appeared as large ring-like regions (15-20 µm in diameter) (Fig. 2A) and consisting of clusters of individual microfilamentous electron dense material between 80 and 120 nm in diameter (Fig. 2B), the podosomes. The outer side of the entire ring-like region was found delimited by microfilaments bundles (black arrow in Fig. 2B). As expected, the rosettes were detected at the cell ventral surface contacting the substrate, as observed in consecutive thin sections cut parallel and very close to the adhesion surface of the culture dish. The rosette stands behind the leading edge of the cell as emphasized by the phase contrast image (Fig. 2A). Higher magnification revealed podosomes of various sizes and shapes containing densely packed and highly branched network of actin filaments.

High magnification images of individual podosomes allowed us to observe mainly two types of arrangements: dots that were resolved as a ring-like arragement of microfilaments exhibiting an electron sparse central region around 25nm (Fig. 2C, red arrowheads in levels 1 and 2), and more electron dense entities evoking transversally sectioned actin bundles (Fig. 2C, level 3). The two types of arrangements can coexist within the same podosome with a tendency to observe the ring arrangement at the level closest to the substratum. Thus, the inner architecture of endothelial podosomes is reminiscent of that observed in Src-transformed cell podosomes for which Marchisio's group described glove finger invaginations originating from the ventral plasma membrane at sites of close contacts (Nitsch et al., 1989).

Endothelial podosomes present similarities and differences with macrophage podosomes

The podosome cap is a recently discovered podosomal substructure that has been revealed in macrophages (Cervero et al., 2018). All data collected so far point to a regulatory function in actomyosin-based contractility. Identified cap components, LSP1, FMNL1, INF2 and SVIL, are involved in the regulation of unbranched actin filaments and of myosin IIA. Although, the existence of a cap structure on the top of podosomes formed in ECs is intuitive, it remains speculative. To explore this issue, we focused on INF2 which is a crucial regulator of podosome *de novo* formation and size and a regulator of contractile events at individual podosomes in macrophages (Panzer et al., 2016). Imaging INF2/F-actin/cortactin triple stained TGFβ-stimulated BAE cells showed that INF2 signal is detected at a higher focal plan compared to F-actin and cortactin, consistent with a cap position (Fig. 3A-D, Suppl. Fig. 3). Thus, similar to isolated and interconnected podosomes in macrophages, rosette-assembled podosomes are capped by an INF2-containing substructure.

Both invadopodia and podosomes are enriched in proteins that regulate actin polymerization including proteins involved in N-WASp/WASp-dependent Arp2/3-complex activation. Nck1 and Grb2 are upstream regulators of this pathway, but whereas Nck1 specifically localizes to invadopodia in breast carcinoma cells, Grb2 specifically localises to podosomes that form in venous ECs (HUVEC cells derived from the human umbilical cord) stimulated with the PKC activator PMA (Oser et al., 2011). In contrast, neither Nck, nor Grb2 are detected at macrophage podosomes (Oser et al., 2011). Data presented in Fig. 3E show that Grb2 localizes to TGFβ-induced podosomes in BAE cells. These results confirm that Grb2 is a component of endothelial podosomes induced by a physiological stimulus.

Reduced oxygen levels stimulate podosome formation in aortic endothelial cells

For convenience, cells are cultured in atmospheric air and podosome formation in cultured cells is assessed under these conditions ("normoxia", 21% O_2). Blood leaving the lungs, via the pulmonary

veins, is pumped by the heart into the arterial system via the aorta. The PO_2 of the newly oxygenated blood is reduced (7% O_2) as compared to that of the lung alveolus (13% O_2) and decreases further downstream of the vascular tree. This raises the question of podosome formation under physiological PO_2. To address this point, we seeded cells at high confluence to obtain a monolayer and in these conditions, TGFβ-induced podosome formation is reduced (Varon et al., 2006). The cultures were exposed to reduced O_2 atmosphere (3% O_2) in a chamber that accurately maintains and controls oxygen levels (as well as maintaining temperature, humidity and CO_2). In contrast to unstimulated cultures in normoxia, podosomes were detected under hypoxia performed in parallel conditions (Fig. 4A, B). Hypoxia-induced podosomes were associated with only a mild increase in gelatinolytic activity (Fig. 4A-C) suggesting that these podosomes were not fully competent for matrix degradation. Interestingly, most superstructures detected were podosome clusters and only occasionally podosome rings, suggesting that podosome dynamics could be altered by O_2 levels. Regarding the response to TGFβ, podosome induction observed under normoxia did not occur under hypoxia, at either TGFβ concentration tested, suggesting that cells become unresponsive to TGFβ signals at low O_2 concentrations. The differences between hypoxia induced podosomes and TGFβ-induced podosomes in terms of gelatinolytic activity may reflect differences in podosome rosette dynamics, ECM degrading enzyme release or cell motility. To examine the influence of O_2 rarefaction in the native endothelium, living arterial vessel segments (carotid artery) were excised from anesthetized mice, opened up along their long axis (Rottiers et al., 2009) and exposed to reduced O_2 concentration. After 24h, samples were fixed, double stained for F-actin/cortactin, nuclei were highlighted with Hoescht and the endothelium was viewed “en face”. Podosome rosettes were induced by exposing the vessel segment to low O_2 concentration (Fig. 4D), confirming that the organelles also form in ischemic endothelial tissues (Fey et al., 2016). When the vessels were fixed *in vivo*, we observed very few if any podosome rosettes in the endothelium (Suppl. Fig. 4). These data establish that the native endothelium of the carotid artery is virtually devoid of podosomes *in vivo* and rule out the possibility that podosomes may have been suppressed by normoxia *ex vivo*. Collectively, these results indicate that hypoxia mitigates TGFβ stimulatory action for podosome induction and that low oxygenated blood is likely to promote podosome assembly in aortic ECs *in vivo.*

Flow stimulates podosome formation in aortic endothelial cells

A primary signal for arterial remodeling is shear stress, which is the frictional force at the endothelial surface produced by flowing blood. Indeed, increase in blood flow increases local shear stress and stimulates arterial diameter expansion which is essential for collateral growth following ischemia (Carmeliet, 2000). We therefore undertook to examine if and how podosome form in BAE cells cultured under shear stress. We took advantage of a set up that uses an orbital shaker to apply shear stress on confluent BAE cells set in tissue-culture dishes. This technique creates a system where the

shear stress experienced by cells at the edge of the dish is laminar and unidirectional, in line with shear stress experienced by ECs in straight and unbranched arteries (Potter et al., 2011). Cells at the edge therefore adopted an elongated and aligned phenotype (Fig. 5A). Cells prepared in the same way but cultured under static conditions did not exhibit any particular phenotype, they were cobblestone and not-aligned in any direction (Fig. 5A). In contrast to unstimulated cultures in the static situation, podosome rosettes were detected under flow conditions (Fig. 5A, B). When TGFβ was added to shear stress-exposed cells, the podosome response was more vigorous than in the control static condition indicating an additive effect of the stimuli (Fig. 5B, C). Of note that superstructures mainly presented as clusters and not rings suggesting that the dynamics of the super-structure was altered by shear stress. These results are consistent with the arterial remodeling that occurs in response to flow and TGFβ (Sho et al., 2003).

Endothelial podosome architecture in 3D contexts

In the quiescent vessel, the endothelium rests on the basement membrane composed of a tightly cross-linked collagen-IV network in which a less dense self-assembled laminin network is connected via entactin (nidogen) and perlecan molecules. Since basement membranes are very thin and basically 2D, podosome studies performed on planar surfaces are to some extent relevant to *in vivo* situations addressing the crossing of this physiological barrier (Rottiers et al., 2009). However, podosome-mediated gaps in the basement membrane (Rottiers et al., 2009) open the way to EC invasion into surrounding tissues. To visualise the podosome forming in ECs confronted by a 3D situation, BAE cells were embedded into a collagen-I (Col-I) preparation in the presence of TGFβ, the mixture was plated onto a glass bottom dish and allowed to gel. The samples were next fixed and stained for podosome markers and with an antibody detecting Col-I breakdown. This antibody, Col1-3/4C_{short}, recognizes a neoepitope of the 3/4 fragment of Col-I created through cleavage by collagenases, such as MT1-MMP (Wolf and Friedl, 2005). Representative images (Fig. 6) show that cells away of the substratum remained suspended in the gel (Fig. 6A) and exhibited elongated protrusions with bulging tips (Fig. 6B). By the time the Col-I was gelling, some cells had sedimented and attached to the bottom of the dish (2D surface), and these cells exhibited the expected podosome rosettes (Fig. 6C). The staining with the Col1-3/4C_{short} antibody confirmed a robust collagenolytic activity that correlated with an increased number of F-actin/cortactin positive globular structures. In the vicinity of these globular structures, the Col1-3/4C_{short} staining authenticated them as *bona fide* podosomes (white arrows). At the rear of a cell, the Col1-3/4C_{short} staining revealed the route of the invading cell (Fig. 6D). When TGFβ was omitted, ECs adopted a more spherical shape and although some protrusions might occasionally develop, they did not present bulged ends nor did they stain for podosome markers (Fig. 6E). In addition, the Col1-3/4C_{short} was barely detected in the cell vicinity, indicating no Col-I cleavage in these samples (Fig. 6E). Thus, TGFβ induces the formation of endothelial podosomes in a

compliant 3D Col-I matrix, but their architecture (globular) and arrangement (along cell protrusions) markedly differed from those observed in the 2D setting (rosettes). In conclusion, in 3D Col-I gels, podosome components cluster along random cell protrusions to form 3D podosomes resembling those described in microvascular ECs invading 3D matrigel (Spuul et al., 2016b) or in macrophages embedded in Col-I gels (Van Goethem et al., 2011).

Conclusions

At the interface between blood and tissues, ECs adapt continuously their functions to respond to microenvironmental changes from the blood and underlying matrix. In physiological contexts, TGFβ signals mediates aortic enlargement, a process driven by ECs, mediated by flow and involving metalloproteinases (MMPs) (Masuda et al., 2003; Sho et al., 2003; Sho et al., 2002b). *In vitro*, TGFβ is a master regulator of podosome formation in aortic ECs. We provide evidence that the composition of the ECM proteins regulate podosome formation in ECs when the cells are co-stimulated with TGFβ but not on their own. In addition, we also show that flow promotes this TGFβ-induced podosome response. Thus, in ECs, podosome formation responds to the coordination of various stimuli. *Ex vivo*, TGFβ-induced endothelial podosomes degrade the underlying basement membrane barrier. The present study reveals that mild hypoxia also promotes podosome formation *in vitro* and *ex vivo*. *In vitro*, hypoxia promotes podosome formation but these podosome have low matrix-degrading capacities. Our studies show that TGFβ in the one hand or flow in the other hand, stimulates matrix proteolysis. It thus appears likely that hypoxia, TGFβ and flow regulate vascular remodeling in a concerted manner. Altogether, these findings suggest that podosome matrix degrading activities concentrated at podosome rosettes enable vessel diameter to increase and this results in an adaptation of the vessel diameter to wall shear stress. Collectively, our results suggest that the podosome rosette is an endothelial cell device devoted to vessel remodeling.

Thus, in addition to TGFβ (Rottiers et al., 2009; Varon et al., 2006), microRNA-155 (Curado et al., 2014), or mechanical constraints (Spuul et al., 2015), flow and hypoxia are identified as two other regulators of podosome formation in arterial ECs. Dimensionality regulates podosome architecture and arrangement. ECs confronted by a 3D environment, elongate and assemble globular-shaped collagenolytic podosomes along cellular extensions that are suggestive of an invading cell (Spuul et al., 2016a). Podosome assembly in response to TGFβ is likely to be modulated by multiple extracellular cues *in vivo*. Altogether, our findings provide new insights that should help to better address the pathophysiological significance of EC podosomes.

Acknowledgments

The authors wish to thank Dr P. Friedl (Department of Cell Biology, Radboudumc, Nijmegen, Netherlands) for providing Col1-3/4C_{short} antibody and Pr Stefan Linder (Institut fur medizinische

Mikrobiologie, Virologie und Hygiene, Universitatsklinikum Eppendorf, Hamburg, Germany) for cap protein antibodies, Pr J. Mitchell and Dr M Reed (Dept. Cardiothoracic Pharmacology, National Heart and Lung Institute, Imperial College London, UK), for helping with the flow experiment setup. We also thank the animal facilities of the University of Bordeaux. The help of Thierry Dakhli and Laetitia Medan is acknowledged. We also thank Clotilde Billottet, Veronique Veillat and Yasmine Amrani (University of Bordeaux) for preliminary experiments.

Competing Interests

The authors do not disclose any competing interests.

Funding

This research was partly funded by INSERM and by the European Union Seventh Framework Programme (FP7/2007–2013) [grant agreement number FP7-237946 (T3Net) to E.G and by the research grant: « Action Thematique Tranversale » (ATT, project HYPOXCELL of the BxCRM, Bordeaux Consortium of Regenerative Medicine at the University of Bordeaux. Additional funding was from the Ligue contre le Cancer (comité de la Gironde) and Fondation de France. P.S. was supported by a postdoctoral fellowship from the Ligue Nationale contre le Cancer, T. D. by a post-doctoral fellowship from Fondation ARC and F.A. from the Fondation Berthe Fouassier. This work has benefited from the facilities and expertise of the Biophysical and Structural Chemistry platform (BPCS) at IECB, CNRS UMS3033, Inserm US001, University of Bordeaux (http://www.iecb.u-bordeaux.fr/index.php/fr/plateformestechnologiques).

3. Materials and methods

Cells

BAE cells (Cell Systems) were maintained in complete endothelial cell growth medium (EGM-MV; Promocell). Cells were cultured at 37°C in a 5% CO_2 humidified atmosphere unless otherwise indicated, and used between passages three and six. Podosome formation assays were performed by double staining for F-actin/cortactin or F-actin/vinculin over a 24h time period (Varon et al., 2006). Hypoxic cultures were carried out in an Invivo 300 workstation (Ruskinns) set at 3% O_2 (5% CO_2, 37°C, and humidified atmosphere).

Cell transfection and plasmid

Cells were transfected with pmEGFP-Lifeact plasmid (kindly provided by Roland Wedlich-Soldner (Riedl et al., 2008) using the Neon® transfection system (Thermofisher) according to the manufacturer's guidelines (3 µg plasmid/5x10^5 cells using 100 µl Tips). Transfection efficiency

ranged between 10 and 20%. Transfected cells were seeded on glass bottom dishes (MatTek Corporation) and analysed/imaged 24 h after transfection.

Mice

All experiments were carried out in accordance with the National Code of Ethics on Animal Experimentation (French Ministry of Agriculture and Fisheries, Animal Care and Use Certificate #A3312043) and approved by the Committee of Ethics of Bordeaux (#A50120219). For *ex vivo* analysis of the endothelium responses, aortic vessel segments were derived from 6- to 8-week-old C57BL/6j mice (Charles River), which were anesthetized by intraperinoneal (*ip*) administration of a mixture of ketamine (100 mg/kg, Merial) and xylazine (10 mg/kg, Bayer) in 100 µl in a sterile saline solution. Tissue samples were fixed and processed for immunofluorescence as described (Rottiers et al., 2009). For endothelium observation *in vivo*, examination of native tissues was performed after mice had received intracardiac perfusion of first 10 ml PBS to wash out the blood and then 40 ml of a 4% paraformaldehyde solution in PBS. For the intracardiac perfusion a peristaltic pump (Dutscher) was used at a flow rate of 10ml/min.

Reagents

Recombinant human TGFβ was obtained from Biotechne and used at 5 ng/ml and for 24h in all assays unless otherwise indicated. Antibodies against the following proteins were obtained as indicated: Cortactin (#05-180) and Vinculin (#V9264) and INF2 (#HPA008527) from Sigma, Grb2 (#sc-8034) from Santa-cruz. The Col1-3/4C_{short} antibody was a kind gift from Pr P. Friedl (Dept of Cell Biology, Radboudumc, Nijmegen, Netherlands). Alexa Fluor 546-phalloidin, Alexa Fluor 488 or 647-labeled secondary antibodies, gelatin coupled Oregon-488 were purchased from Invitrogen.

Immunofluorescence staining and matrix degradation assay

Subconfluent cells grown on glass coverslips were prepared for immunofluorescence as previously described (Varon et al., 2006). The coverslips were washed in water and mounted on microscope slides with ProLong® Gold *Antifade* containing (or not) 4,6-diamidino-2-phenylindole (DAPI) (Thermofisher). For matrix degradation assay, BAE cells were seeded on coverslips coated with green-fluorescent Oregon Green-488 gelatin (Thermofisher) and stimulated as indicated. Cells were fixed and samples were processed for immunofluorescence to visualize podosome rosettes and matrix degradation. Quantification of degradation areas on fluorescent-labeled gelatin was performed for at least 10 fields (×10 objective lens) for each coverslip. The areas of degradation were quantified by using ImageJ software. Degraded areas were thresholded and measured by Analyze Particles function. The total degradation area (expressed in μm^2) was then normalized for the number of cells (degradation index) in respective fields.

Microscopy and image analysis

Cells and aortic vessel segments were analyzed by confocal imaging using a Zeiss LSM 510 inverted laser-scanning fluorescence microscope equipped with acquisition software (LSM 510 acquisition software; Zeiss) and a ×63 NA 1.4 oil-immersion objective. Quadruple-color imaging using DAPI, Alexa Fluor 488- or Alexa Fluor 647-labeled secondary antibodies, and Alexa Fluor 546-phalloidin (Thermofisher) was obtained using selective laser excitation at 350 nm, 488 nm, 633 nm and 543 nm, respectively. Each channel was imaged sequentially using the multitrack recording module before merging. Fluorescent images were processed with ImageJ. Duplicate coverslips were analysed per condition.

Time-lapse videomicroscopy

For live-cell imaging, BAE cells were seeded in 35-mm nr. 0 glass bottom dishes (MatTek, Ashland, MA), then transferred to observation medium at 37°C. Dishes were placed on a thermostated stage, and cells were imaged with a Zeiss inverted laser-scanning confocal microscope LSM510 and a 63×/NA 1.4 Zeiss Plan-Apochromat oil immersion objective. Live-cell recordings were done with unidirectional scanning, average 1, pinhole 1 AU using selective laser excitation at 488 nm with 10% laser power. Images were acquired every 38 s for specified time and data were analyzed with ImageJ.

Correlative fluorescence and electron microscopy

BAE cells cultured on gridded glass bottom dishes (MatTek Corporation) were treated with TGFβ and immediately fixed with 4% (v/v) formaldehyde and 1% (v/v) glutaraldehyde in phosphate buffer 0.1 M containing 0.25mM $CaCl_2$ and 0.5mM $MgCl_2$, pH 7.4 at room temperature for 2h. They were labelled with Alexa Fluor 488-phalloidin 2U/ml for 30min and examined by epifluorescence to select podosomes and check their position using the grid by phase contrast (invert LEICA DMI 6000 microscope). After that, samples were post-fixed using 1% (v/v) osmium tetroxide and embedded in resin (Epon). Ultra-thin sections (70 nm) of region of interest, were performed on ultramicrotome (RMC, powertome PC), collected on butvar-coated single-slot copper grids and stained with 2% (v/v) uranyl acetate and lead citrate. Grids were examined by TEM (CM120, FEI) and the images were acquired using a digital Gatan camera 2Kx2K.

Application of fluid shear stress

BAE cells were grown to confluence on coverslips attached to the bottom of 6-well plates and flow was applied using an orbital shaker (Heidolph™ Agitateur orbital Rotamax 120), set in a tissue culture incubator (37°C, 5% CO_2) as designed by the group of Jane Mitchell (Potter et al., 2011). Speed was set at 210 rpm to conform with the computational fluid dynamics that were modeled in this study. Arterial magnitude of shear stress (11 dynes/cm^2) was achieved in the periphery of the well (Dardik et al., 2005). After 6 days (the culture medium was replaced once), TGFβ was then added (5ng/ml) for

24h and samples were fixed. Coverslips were gently detached and subjected to immunofluorescence staining and imaging.

3D culture in Col-I gel

A mixture of rat-tail Col-I (BD Biosciences), MEM (life technologies), Sodium Bicarbonate and distilled water was prepared on ice. BAE cells were mixed with this preparation and set onto a glass bottom dish (MatTek device). The mixture was incubated at 37°C for 30-40 min until gelation and the matrix was subsequently neutralised by adding 37°C pre-heated culture medium. Samples were fixed and stained as indicated.

2D culture on ECM matrices.

BAE cells were seeded onto tissue culture coverslips that had been coated with ECM proteins. Coverslip coating was achieved by incubation with ECM proteins diluted in PBS: fibronectin (from human plasma, Corning) at 20 µg/ml for 90 min, 37 ° C; Col-I (from rat tail, BD Biosciences) at 200 µg/ml for 30 min, 37°C; laminin (from human placenta, Sigma) at 20 µg/ml for 60 min, RT; gelatin (from bovine skin, Sigma) at 2% for 30 min, 37°C; vitronectin (from human plasma, Sigma) at 5µg/ml for 1h, RT; Col-IV (from human placenta, Sigma) at 10 µg/ml for 18h, 4°C. Coversplips were rinsed twice with PBS before use.

Statistics

Statistical analysis was performed on GraphPad Prism 8 (GraphPad Software, Inc., San Diego. CA, USA). Quantification values are represented by their mean ± s.d. Significance within or between groups was assessed by using either a one-way or two-way ANOVA followed by Tukey´s or Šídák multiple comparisons test as specified in the figure legends. Differences were considered to be statistically significant at $P<0.05$.

Figure legends

Figure 1: General and specific features of podosomes in aortic endothelial cells

A-C. BAE cells were seeded on glass coverslips and stimulated with 5 ng/ml TGFβ for 24h. Under these conditions, BAE cells have synthesised and secreted adhesive proteins; these and similar proteins present in the serum of the culture medium have adsorbed onto the naked glass. Cells were fixed and triple stained for F-actin, vinculin and Hoechst. A. Podosome rosette is indicated with a white arrow, zoomed area shown in panel (**B**) is indicated with a white box. **B**. Podosome rosette shown in the boxed region in A consists of individual podosomes (indicated with white arrows),

individual stainings are shown on the right. **C**. Podosome cluster is indicated with a white arrow, individual stainings are shown on the right.

D. Live cell imaging of TGFβ stimulated BAE cells expressing Lifeact-mEGFP shows the cycle of the formation of podosome rosette. Zoomed area shown on the right is indicated with a white box, podosome cluster in the beginning of the recording is indicated with white arrow. Scale bars: A, 20 µm; B, 10 µm; C, 20 µm and D, 20µm.

E. BAE cells were seeded on various matrices and stimulated with 5 ng/ml TGFβ for 24h or left untreated (control). Cells were fixed and stained for F-actin/cortactin podosome markers. n=3 individual experiments in which podosomes were scored in 300 cells per condition, mean±s.d. is shown. *P < 0.05; **P < 0.01; ****P < 0.0001 (two-way ANOVA with Šídák multiple comparison test was used). The statistical significance compared to the respective controls and compared to the glass condition is shown.

Figure 2. Ultrastructural characterisation of podosome rosettes formed in BAE cells using correlative fluorescence and electron microscopy

Cells were seeded on gridded glass coverslips and fluorescent staining of the cytoskeleton was performed to detect cells with podosome rosettes.

A. Phase contrast optical microscopy is used to locate the position of a cell with podosome rosetteon the coverslip in order to analyse it by TEM.

B. At low magnification, thin sections cut parallel and very close to the bottom of the culture coverslip, show a large ring-like region, free of membrane bound organelles, consisting of clusters of dense microfilamentous material. The ring-like region outer side is delimited by microfilament bundles (black arrow).

C. Three consecutive thin sections were observed at higher magnification. At the level closest to the substratum (1), in sections (1) and (2), some individual dots are resolved as consisting in an electron sparse area of about 25 nm in diameter, surrounded by a thick rim of microfilaments (red arrowheads and inset from the red boxed region). In the last section going deeper inside the cell (3), dots consist of clusters of transversally sectioned microfilaments. Scale bars, A, 10µm; B, 1µm; C, 1µm and yellow inset, 100 nm.

Figure 3: The cap component INF2 and the adapter protein Grb2 are located in endothelial podosomes.

A. Representative picture of a TGFβ-induced endothelial podosome superstructure triple stained for F-actin (green), cortactin (red) and the cap protein INF2 (magenta). EC nuclei are visualized with Hoechst (blue) (**left panel**). High magnifications images of the region **1** showing the individual and merged channels highlight the colocalization of the 3 different podosome components (**right panels**). Scale bar, 10 µm (**left**) and 2 µm (**right**)

B. Orthogonal views of the z-stack used to generate the picture shown in (**A**) reveal that INF2 signal is detected at a higher focal plane compared to F-actin and cortactin.

C. The graph shows the fluorescence intensity of the three different probes according to their localization along the z axis. Note that the lines for F-actin and cortactin overlap whereas the line for INF2 shows cap-like localization of this protein on top of the F-actin/cortactin core.

D. 3D volume reconstruction of the F-actin (green), cortactin (red) and INF2 (magenta) signals from the area **2** shown in (**B**). Note the typical cap protein localization of the INF2 signal above the F-actin and cortactin signals.

E. High magnification image of a TGFβ-induced endothelial podosome superstructure triple stained for F-actin (green), cortactin (red) and the adapter protein Grb2 (white). EC nuclei are visualized with Hoechst (blue). Scale bar, 10 µm.

Figure 4: Hypoxia stimulates podosome formation in arterial endothelial cells

A. Visualization of podosome rosettes in BAE cells cultured for 48h under standard (21% O_2) or reduced (3% O_2) O_2 concentration, and either left untreated or treated with TGFβ at low (5ng/ml) or high (10 ng/ml) concentrations for the last 24h. **Top panel**: Podosomes double stained for F-actin (red) and cortactin (green) and associated Oregon green-gelatin (grey) matrix degradation. EC nuclei are visualized with Hoechst (blue). **Middle panel**: Areas of gelatin degradation are revealed by the lack of Oregon green fluorescence (black). **Bottom panel:** Podosome superstructures are detected by the F-actin/cortactin colocalization (yellow). Scale bar, 10 µm.

B. Representative low magnification images of Oregon green/hoechst staining showing the cell degradation capability in each experimental situation. Scale bar, 200 µm.

C. Quantification of podosome formation (**left**) and matrix degradation (**right**) in BAE cell cultured under atmospheric or reduced O_2 concentration, and exposed or not to TGFβ. Compared to untreated BAE cells cultured under standard O_2 conditions, cells exposed to reduced O_2 concentrations or stimulated with TGFβ show increased podosome formation and matrix degradation.

Data are representative of 3 independent experiments performed in duplicate. Graphs are presented as mean values ± SD (bars) and individual values (dots). *P < 0.05; **P < 0.01; ***P < 0.001 vs respective control (one-way ANOVA followed by Tukey´s post-tests).

D. Visualization of podosomes in ECs from vessel segments (carotid artery) exposed to atmospheric or reduced O_2 concentration. **Top panel**: Representative staining for F-actin (red) in the 2 situations. **Middle panel**: Representative images of the cortactin staining (green) in the 2 situations. **Bottom panel:** Superposition of the F-actin/cortactin signals (yellow) revealing podosome superstructures in the endothelium from vessel segments exposed to reduced O_2 concentration (white arrowheads). **Right column:** Higher magnification of the endothelium in the boxed region shown in the middle column, revealing the typical organization of podosomes in a rosette. Scale bar, 40 µm (**middle** and **left column**) and 5 µm (**right column**).

Figure 5: Shear stress stimulates podosome formation in aortic endothelial cells

A. Morphology of confluent untreated and TGFβ-treated BAE cultures under either static conditions or exposed to an arterial shear stress of 11 dyne/cm^2 for 7 days. The phase contrast images (**top panel**) and the F-actin/Hoechst double staining (**bottom panel**) confirm EC elongation and alignment along the direction of flow. Scale bar, 150 µm.

B. Podosomes triple stained for F-actin (green), cortactin (white) and vinculin (red). Low magnification images (**top panel**) show the typical localization of podosome clusters away from the EC nucleus (revealed with Hoechst, blue). High magnifications images (**bottom panel**) of the individual and merged channels show the colocalization of the 3 different podosome components. Scale bar, 30 µm.

C. Quantification of podosome formation in cells exposed or not to flow and in absence or presence of TGFβ. Compared to untreated BAE cells cultured under static conditions, cells exposed to flow and cells stimulated with TGFβ show increased podosome formation. The data also reveal a synergistic effect of TGFβ and flow on the formation of podosomes.
Data are representative of 3 independent experiments performed in duplicate. Graphs are presented as mean values ± SD (bars) and individual values (dots). **P < 0.01; ***P < 0.001 vs respective control (one-way ANOVA followed by Tukey´s post-tests).

Figure 6: In 3D collagen gels, TGFβ-stimulated ECs form protrusions with globular 3D podosomes and Col-I breakdown is increased.

A. TGFβ-treated BAE cells suspended in a Col-I gel, stained with F-actin/cortactin and Hoechst. Scale bar, 30 µm.

B. High magnification of the boxed cell in (**A**) showing the elongated morphology, the protrusions and 3D podosomes under 3 different angles. Scale bar, 30 µm.

C. Cells that have reached the 2D surface during the gelation period have assembled podosome rosettes (white arrowhead), cells suspended in the Col-I gel display globular podosomes (magenta arrowheads). Scale bar, 30 µm.

D. Col1 3/4C_{short} antibody staining reveals Col-I cleavage by TGFβ-stimulated BAE cells in 3D. Images have been reconstructed in 3D using the Imaris software (mode blend and mix). In blend mode (black background), F-actin is shown in red, cortactin in green, nuclei in blue and 3D podosomes are highlighted by white arrows. Images in mix mode (white background) show F-actin in red, cortactin in white, cleaved collagen in green, nuclei in blue and 3D podosomes are highlighted by black arrows. Scale bar, 30 µm.

E. Col1 3/4C_{short} antibody staining reveals barely detectable Col-I cleavage signals in unstimulated BAE cells in 3D. Scale bar, 10 µm.

Suppl. Figure 1: Dynamics of podosome rosettes.

TGFβ stimulated BAE cells expressing Lifeact-mEGFP were analysed with interference reflection microscopy (IRM) during live cell imaging. Podosome rosettes (indicated with a white arrow) are visualised with Lifeact-mEGFP showing an average diameter of 14.73 µm ± 62.3 µm (n=10). Dark area on IRM images (indicated with a black arrow) illustrates the closeness podosome rosette area to the glass coverslip. Zoomed areas shown on the right are indicated with a boxed regions in the beginning of the recording. Snapshots from one podosome rosette cycle is illustrated, upper zoomed images show Lifeact-mEGFP and lower ones respective IRM images. Scale bars: 20 µm;

Suppl. Figure 2: Podosome rosettes degrade the underlying gelatin matrix.

A. BAE cells on Oregon Green-488 conjugated gelatin were stimulated with 5 ng/ml TGFβ for 24h. Cells were fixed and stained for F-actin and Hoechst. Degraded areas were seen as dark holes in gelatin layer having an average diameter of 18.09 µm ± 6.9 µm (n=68). Scale bar, 20 µm;

B. Graph showing a significant increase in the degradation index (degraded area per cell) after TGFβ stimulation. n=3 independent experiments in which 10 fields (1500 cells) were analysed per experimental point, mean±s.d. is shown. **P<0.01 (Student´s t-test was used). Video 1. Live cell

imaging of TGFβ stimulated BAE cell expressing Lifeact-mEGFP shows the cycle of the formation of podosome rosette. Images were acquired every 38 s and playback is 10 fps. Scale bar, 20 µm.

Suppl. Figure 3: The cap component INF2 localizes on top of endothelial podosomes.

A. Representative picture of a TGFβ-induced endothelial podosome superstructure triple stained for F-actin (green), cortactin (red) and the cap protein INF2 (magenta). EC nuclei are visualized with Hoechst (blue). Scale bar, 10 µm.

B. Consecutive optical sections from the z-stack used to generate the picture shown in (**A**) reveal that INF2 signal is detected at a higher focal plane compared to F-actin and cortactin.

C. 3D volume reconstruction of the F-actin (green), cortactin (red) and INF2 (magenta) signals from the z-stack file shown in (**A**) and (**B**). Note the typical cap protein localization of the INF2 signal above the F-actin and cortactin signals. The arrowheads points at the area observed from (**B**).

Suppl. Figure 4: The arterial endothelium is devoid of podosome rosette *in vivo*
Visualization of the arterial endothelium from a vessel segment (carotid artery) excised after fixation by *in vivo* perfusion. Representative staining for F-actin (red), cortactin (green) and superposition of the two signals (yellow) showing the colocalisation of F-actin and cortactin at the endothelial cell cortex in the endothelium monolayer. Note the absence of typical ring-like staining (podosome rosette) in ECs. EC nuclei are visualized with Hoechst (blue). Scale bar, 40 µm.

References

Aga M, Bradley JM, Keller KE, Kelley MJ, Acott TS. 2008. Specialized podosome- or invadopodia-like structures (PILS) for focal trabecular meshwork extracellular matrix turnover. Invest Ophthalmol Vis Sci 49(12):5353-5365.

Akisaka T, Yoshida H, Suzuki R, Takama K. 2008. Adhesion structures and their cytoskeleton-membrane interactions at podosomes of osteoclasts in culture. Cell Tissue Res 331(3):625-641.

Alonso F, Spuul P, Daubon T, Kramer I, Genot E. 2019. Variations on the theme of podosomes: A matter of context. Biochimica et biophysica acta Molecular cell research 1866(4):545-553.

Basson CT, Kocher O, Basson MD, Asis A, Madri JA. 1992. Differential modulation of vascular cell integrin and extracellular matrix expression in vitro by TGF-beta 1 correlates with reciprocal effects on cell migration. J Cell Physiol 153(1):118-128.

Branch KM, Hoshino D, Weaver AM. 2012. Adhesion rings surround invadopodia and promote maturation. Biol Open 1(8):711-722.

Buccione R, Orth JD, McNiven MA. 2004. Foot and mouth: podosomes, invadopodia and circular dorsal ruffles. Nat Rev Mol Cell Biol 5(8):647-657.

Burgstaller G, Gimona M. 2004. Actin cytoskeleton remodelling via local inhibition of contractility at discrete microdomains. J Cell Sci 117(Pt 2):223-231.
Calle Y, Burns S, Thrasher AJ, Jones GE. 2006. The leukocyte podosome. Eur J Cell Biol 85(3-4):151-157.
Carmeliet P. 2000. Mechanisms of angiogenesis and arteriogenesis. Nat Med 6(4):389-395.
Cervero P, Wiesner C, Bouissou A, Poincloux R, Linder S. 2018. Lymphocyte-specific protein 1 regulates mechanosensory oscillation of podosomes and actin isoform-based actomyosin symmetry breaking. Nat Commun 9(1):515.
Collin O, Tracqui P, Stephanou A, Usson Y, Clement-Lacroix J, Planus E. 2006. Spatiotemporal dynamics of actin-rich adhesion microdomains: influence of substrate flexibility. J Cell Sci 119(Pt 9):1914-1925.
Curado F, Spuul P, Egana I, Rottiers P, Daubon T, Veillat V, Duhamel P, Leclercq A, Gontier E, Genot E. 2014. ALK5 and ALK1 play antagonistic roles in transforming growth factor beta-induced podosome formation in aortic endothelial cells. Mol Cell Biol 34(24):4389-4403.
Dardik A, Chen L, Frattini J, Asada H, Aziz F, Kudo FA, Sumpio BE. 2005. Differential effects of orbital and laminar shear stress on endothelial cells. J Vasc Surg 41(5):869-880.
Fey T, Schubert KM, Schneider H, Fein E, Kleinert E, Pohl U, Dendorfer A. 2016. Impaired endothelial shear stress induces podosome assembly via VEGF up-regulation. FASEB J 30(8):2755-2766.
Fuller K, Ross JL, Szewczyk KA, Moss R, Chambers TJ. 2010. Bone is not essential for osteoclast activation. PLoS One 5(9).
Han H, Kampik D, Grehn F, Schlunck G. 2013. TGF-beta2-induced invadosomes in human trabecular meshwork cells. PLoS One 8(8):e70595.
Kaverina I, Stradal TE, Gimona M. 2003. Podosome formation in cultured A7r5 vascular smooth muscle cells requires Arp2/3-dependent de-novo actin polymerization at discrete microdomains. J Cell Sci 116(Pt 24):4915-4924.
Kuo SL, Chen CL, Pan YR, Chiu WT, Chen HC. 2018. Biogenesis of podosome rosettes through fission. Sci Rep 8(1):524.
Labernadie A, Thibault C, Vieu C, Maridonneau-Parini I, Charriere GM. 2010. Dynamics of podosome stiffness revealed by atomic force microscopy. Proc Natl Acad Sci U S A 107(49):21016-21021.
Linder S, Aepfelbacher M. 2003. Podosomes: adhesion hot-spots of invasive cells. Trends Cell Biol 13(7):376-385.
Luxenburg C, Winograd-Katz S, Addadi L, Geiger B. 2012. Involvement of actin polymerization in podosome dynamics. J Cell Sci 125(Pt 7):1666-1672.
Masuda H, Kawamura K, Nanjo H, Sho E, Komatsu M, Sugiyama T, Sugita A, Asari Y, Kobayashi M, Ebina T, Hoshi N, Singh TM, Xu C, Zarins CK. 2003. Ultrastructure of endothelial cells under flow alteration. Microsc Res Tech 60(1):2-12.
Murphy DA, Diaz B, Bromann PA, Tsai JH, Kawakami Y, Maurer J, Stewart RA, Izpisua-Belmonte JC, Courtneidge SA. 2011. A Src-Tks5 pathway is required for neural crest cell migration during embryonic development. PLoS One 6(7):e22499.
Nitsch L, Gionti E, Cancedda R, Marchisio PC. 1989. The podosomes of Rous sarcoma virus transformed chondrocytes show a peculiar ultrastructural organization. Cell biology international reports 13(11):919-926.
Oser M, Dovas A, Cox D, Condeelis J. 2011. Nck1 and Grb2 localization patterns can distinguish invadopodia from podosomes. Eur J Cell Biol 90(2-3):181-188.
Pan YR, Chen CL, Chen HC. 2011. FAK is required for the assembly of podosome rosettes. J Cell Biol 195(1):113-129.
Panzer L, Trube L, Klose M, Joosten B, Slotman J, Cambi A, Linder S. 2016. The formins FHOD1 and INF2 regulate inter- and intra-structural contractility of podosomes. J Cell Sci 129(2):298-313.
Patel A, Dash PR. 2012. Formation of atypical podosomes in extravillous trophoblasts regulates extracellular matrix degradation. Eur J Cell Biol 91(3):171-179.
Paterson EK, Courtneidge SA. 2018. Invadosomes are coming: new insights into function and disease relevance. FEBS J 285(1):8-27.

Potter CM, Lundberg MH, Harrington LS, Warboys CM, Warner TD, Berson RE, Moshkov AV, Gorelik J, Weinberg PD, Mitchell JA. 2011. Role of shear stress in endothelial cell morphology and expression of cyclooxygenase isoforms. Arterioscler Thromb Vasc Biol 31(2):384-391.

Riedl J, Crevenna AH, Kessenbrock K, Yu JH, Neukirchen D, Bista M, Bradke F, Jenne D, Holak TA, Werb Z, Sixt M, Wedlich-Soldner R. 2008. Lifeact: a versatile marker to visualize F-actin. Nat Methods 5(7):605-607.

Rottiers P, Saltel F, Daubon T, Chaigne-Delalande B, Tridon V, Billottet C, Reuzeau E, Genot E. 2009. TGFbeta-induced endothelial podosomes mediate basement membrane collagen degradation in arterial vessels. J Cell Sci 122(Pt 23):4311-4318.

Santiago-Medina M, Gregus KA, Nichol RH, O'Toole SM, Gomez TM. 2015. Regulation of ECM degradation and axon guidance by growth cone invadosomes. Development 142(3):486-496.

Schachtner H, Calaminus SD, Sinclair A, Monypenny J, Blundell MP, Leon C, Holyoake TL, Thrasher AJ, Michie AM, Vukovic M, Gachet C, Jones GE, Thomas SG, Watson SP, Machesky LM. 2013. Megakaryocytes assemble podosomes that degrade matrix and protrude through basement membrane. Blood 121(13):2542-2552.

Sho E, Komatsu M, Sho M, Nanjo H, Singh TM, Xu C, Masuda H, Zarins CK. 2003. High flow drives vascular endothelial cell proliferation during flow-induced arterial remodeling associated with the expression of vascular endothelial growth factor. Exp Mol Pathol 75(1):1-11.

Sho E, Sho M, Singh TM, Nanjo H, Komatsu M, Xu C, Masuda H, Zarins CK. 2002a. Arterial enlargement in response to high flow requires early expression of matrix metalloproteinases to degrade extracellular matrix. Exp Mol Pathol 73(2):142-153.

Sho M, Sho E, Singh TM, Komatsu M, Sugita A, Xu C, Nanjo H, Zarins CK, Masuda H. 2002b. Subnormal shear stress-induced intimal thickening requires medial smooth muscle cell proliferation and migration. Exp Mol Pathol 72(2):150-160.

Spuul P, Chi PY, Billottet C, Chou CF, Genot E. 2015. Microfluidic devices for the study of actin cytoskeleton in constricted environments: Evidence for podosome formation in endothelial cells exposed to a confined environment. Methods.

Spuul P, Chi PY, Billottet C, Chou CF, Genot E. 2016a. Microfluidic devices for the study of actin cytoskeleton in constricted environments: Evidence for podosome formation in endothelial cells exposed to a confined slit. Methods 94:65-74.

Spuul P, Daubon T, Pitter B, Alonso F, Fremaux I, Kramer I, Montanez E, Genot E. 2016b. VEGF-A/Notch-Induced Podosomes Proteolyse Basement Membrane Collagen-IV during Retinal Sprouting Angiogenesis. Cell Rep 17(2):484-500.

van den Dries K, Meddens MB, de Keijzer S, Shekhar S, Subramaniam V, Figdor CG, Cambi A. 2013. Interplay between myosin IIA-mediated contractility and actin network integrity orchestrates podosome composition and oscillations. Nat Commun 4:1412.

van den Dries K, Nahidiazar L, Slotman JA, Meddens MBM, Pandzic E, Joosten B, Ansems M, Schouwstra J, Meijer A, Steen R, Wijers M, Fransen J, Houtsmuller AB, Wiseman PW, Jalink K, Cambi A. 2019. Modular actin nano-architecture enables podosome protrusion and mechanosensing. Nat Commun 10(1):5171.

van den Dries K, van Helden SF, te Riet J, Diez-Ahedo R, Manzo C, Oud MM, van Leeuwen FN, Brock R, Garcia-Parajo MF, Cambi A, Figdor CG. 2012. Geometry sensing by dendritic cells dictates spatial organization and PGE(2)-induced dissolution of podosomes. Cell Mol Life Sci 69(11):1889-1901.

van den Dries K, van Helden SF, te Riet J, Diez-Ahedo R, Manzo C, Oud MM, van Leeuwen FN, Brock R, Garcia-Parajo MF, Cambi A, Figdor CG. 2012. Geometry sensing by dendritic cells dictates spatial organization and PGE(2)-induced dissolution of podosomes. Cell Mol Life Sci 69(11):1889-1901.

Van Goethem E, Guiet R, Balor S, Charriere GM, Poincloux R, Labrousse A, Maridonneau-Parini I, Le Cabec V. 2011. Macrophage podosomes go 3D. Eur J Cell Biol 90(2-3):224-236.

Varon C, Tatin F, Moreau V, Van Obberghen-Schilling E, Fernandez-Sauze S, Reuzeau E, Kramer I, Genot E. 2006. Transforming growth factor beta induces rosettes of podosomes in primary aortic endothelial cells. Mol Cell Biol 26(9):3582-3594.

Veillat V, Spuul P, Daubon T, Egana I, Kramer I, Genot E. 2015. Podosomes: Multipurpose organelles? Int J Biochem Cell Biol 65:52-60.

Wolf K, Friedl P. 2005. Functional imaging of pericellular proteolysis in cancer cell invasion. Biochimie 87(3-4):315-320.

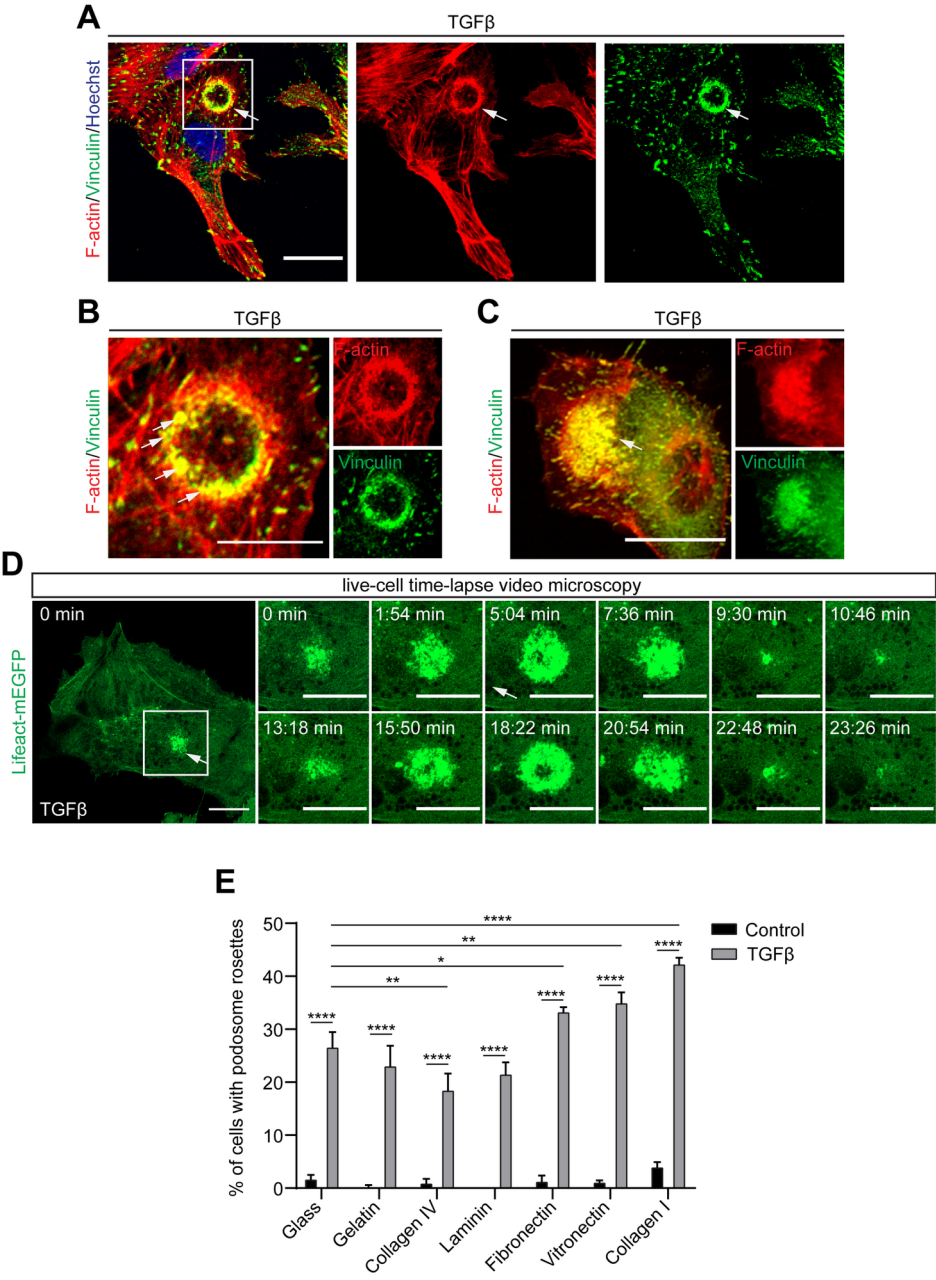
A
TGFβ
F-actin/Vinculin/Hoechst
B
TGFβ
F-actin/Vinculin
F-actin
Vinculin
C
TGFβ
F-actin/Vinculin
F-actin
Vinculin
D
live-cell time-lapse video microscopy
Lifeact-mEGFP
0 min
TGFβ
0 min
1:54 min
5:04 min
7:36 min
9:30 min
10:46 min
13:18 min
15:50 min
18:22 min
20:54 min
22:48 min
23:26 min
E
% of cells with podosome rosettes
Control
TGFβ
Glass
Gelatin
Collagen IV
Laminin
Fibronectin
Vitronectin
Collagen I

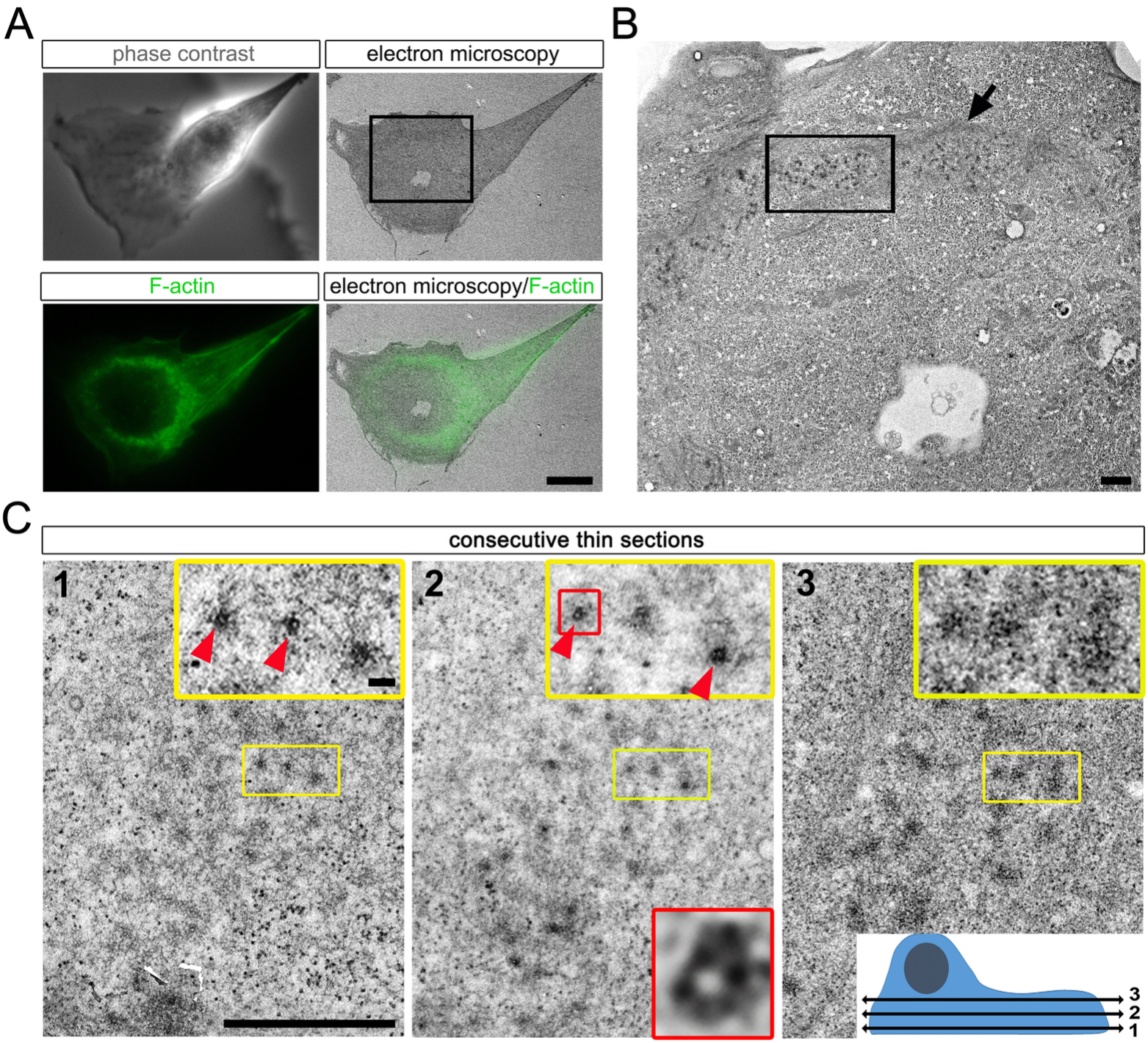
A
phase contrast
electron microscopy
F-actin
electron microscopy/F-actin
B
C
consecutive thin sections
1
2
3
3
2
1

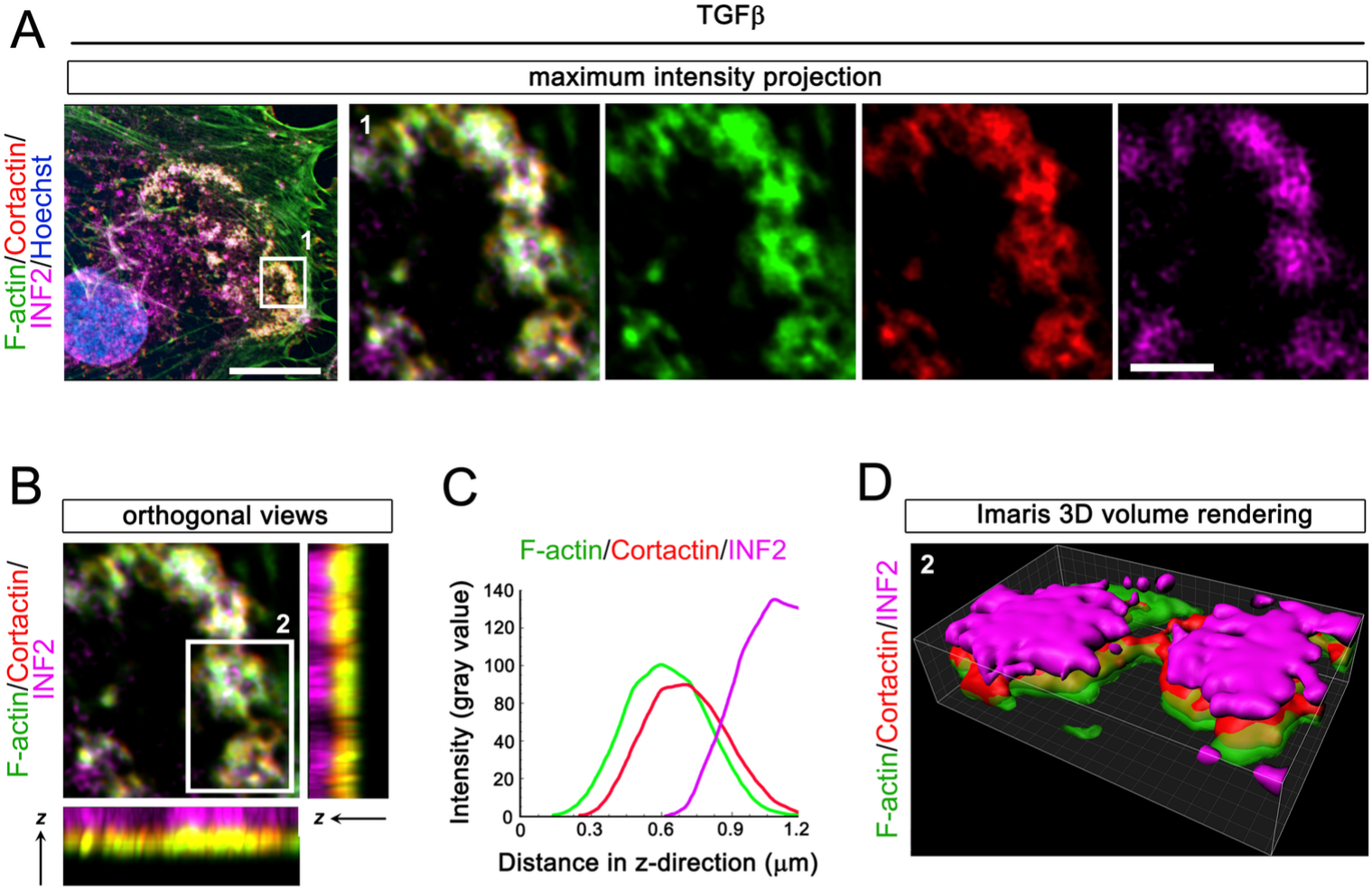
A
TGFβ
maximum intensity projection
F-actin/Cortactin/
INF2/Hoechst
1
1
B
orthogonal views
F-actin/Cortactin/
INF2
2
z
z
C
F-actin/Cortactin/INF2
Intensity (gray value)
140
120
100
80
40
20
0
0
0.3
0.6
0.9
1.2
Distance in z-direction (μm)
D
Imaris 3D volume rendering
F-actin/Cortactin/INF2
2
E
TGFβ
F-actin/Cortactin/
Grb2/Hoechst

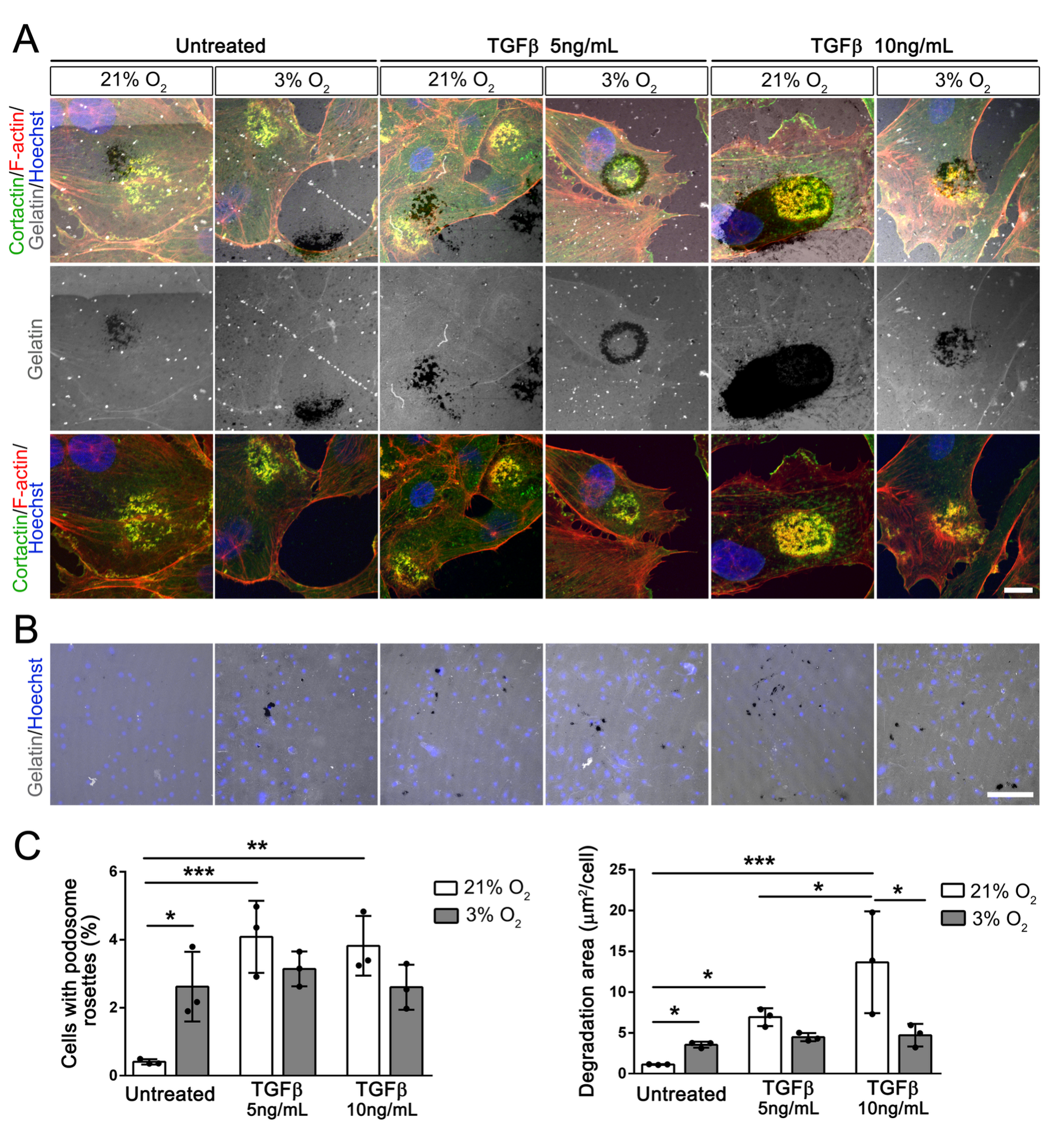
A
Untreated
TGFβ 5ng/mL
TGFβ 10ng/mL
21% O2
3% O2
21% O2
3% O2
21% O2
3% O2
Cortactin/F-actin/
Gelatin/Hoechst
Gelatin
Cortactin/F-actin/
Hoechst
B
Gelatin/Hoechst
C
Cells with podosome rosettes (%)
0
2
4
6
*
***
**
21% O2
3% O2
Untreated
TGFβ 5ng/mL
TGFβ 10ng/mL
Degradation area (μm²/cell)
0
5
10
15
20
25
*
*
*
***
21% O2
3% O2
Untreated
TGFβ 5ng/mL
TGFβ 10ng/mL

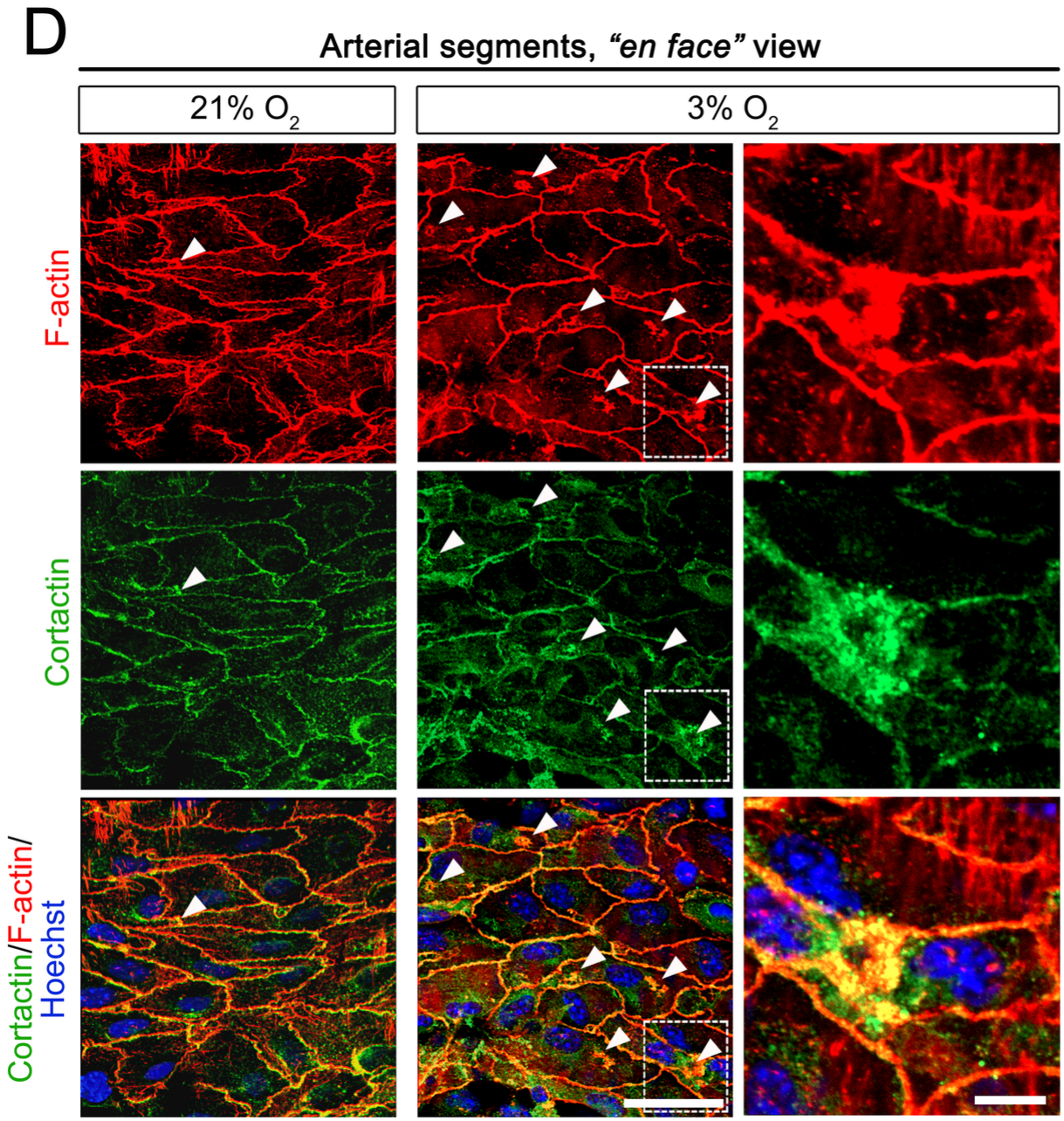
D
Arterial segments, "en face" view
21% O2
3% O2
F-actin
Cortactin
Cortactin/F-actin/
Hoechst

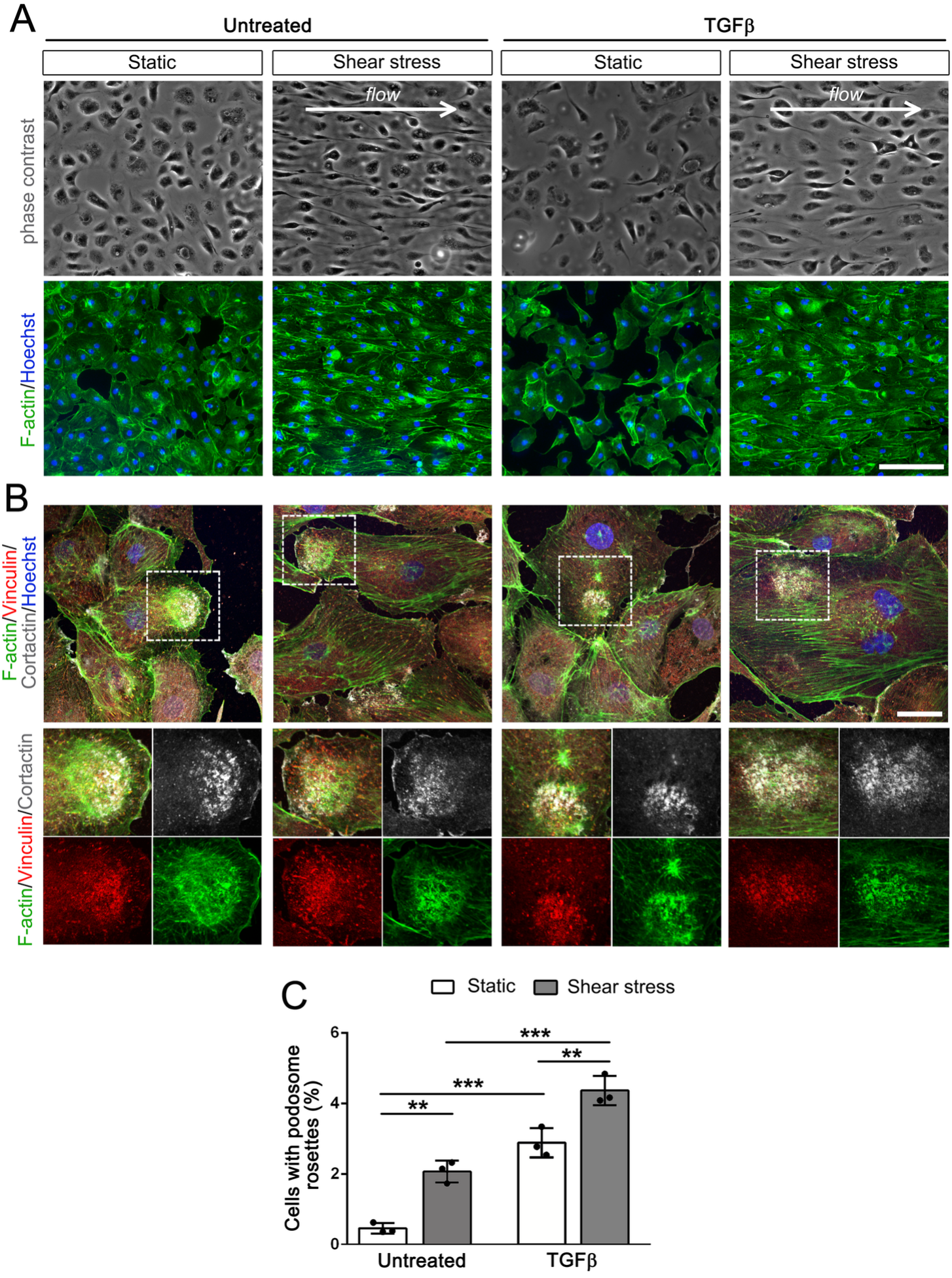
A
Untreated
TGFβ
Static
Shear stress
Static
Shear stress
flow
flow
phase contrast
F-actin/Hoechst
B
F-actin/Vinculin/
Cortactin/Hoechst
F-actin/Vinculin/Cortactin
C
Static
Shear stress
Cells with podosome rosettes (%)
0
2
4
6
**
***
***
**
Untreated
TGFβ

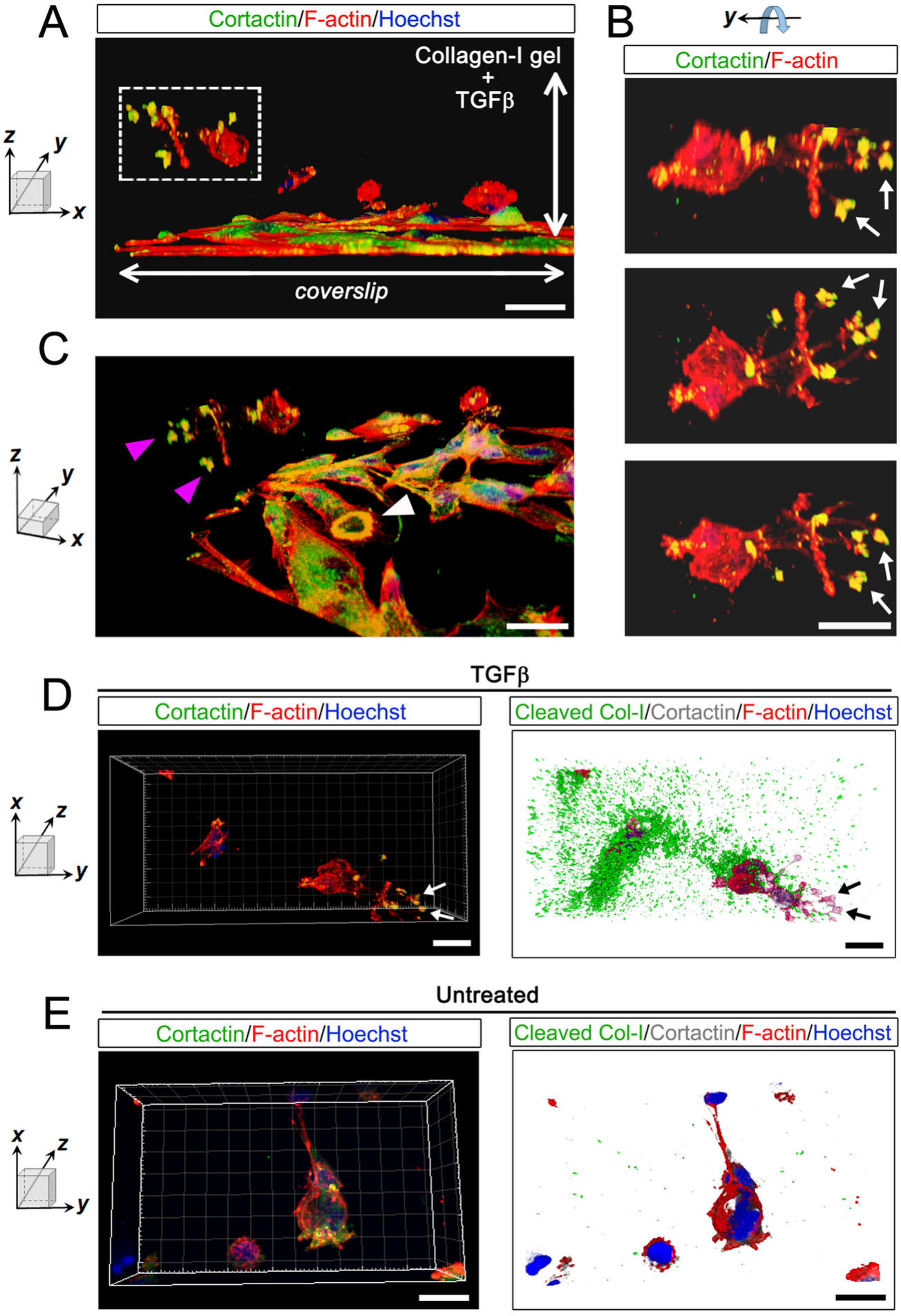
A
Cortactin/F-actin/Hoechst
Collagen-I gel
+
TGFβ
coverslip
z
y
x
B
y
Cortactin/F-actin
C
D
TGFβ
Cortactin/F-actin/Hoechst
Cleaved Col-I/Cortactin/F-actin/Hoechst
E
Untreated
Cortactin/F-actin/Hoechst
Cleaved Col-I/Cortactin/F-actin/Hoechst